

Trapped-ion toolbox to simulate quantum Otto heat engines

Rogério Jorge de Assis,¹ Ciro Micheletti Diniz,¹ Norton Gomes de Almeida,² and Celso Jorge Villas-Bôas¹

¹*Departamento de Física, Universidade Federal de São Carlos, 13.565-905, São Carlos - SP, Brazil*

²*Instituto de Física, Universidade Federal de Goiás, 74.690-900, Goiânia - GO, Brazil*

We present a scheme that utilizes an ion confined within a bi-dimensional trap to simulate a quantum Otto heat engine whose working substance is a two-level system. In this scheme, the electronic component of the ion (the two-level system) can interact with effective heat reservoirs of different types. We specifically focus on effective thermal reservoirs (those with positive temperatures), effective heat reservoirs with apparent negative temperatures, and effective squeezed thermal reservoirs. We show how to generate these effective reservoirs and provide numerical results to illustrate the applicability of the presented scheme. Finally, considering the same types of effective heat reservoirs, we briefly discuss the simulation of a quantum Otto heat engine where a quantum harmonic oscillator serves as the working substance.

I. INTRODUCTION

In recent decades, researchers have been actively working on formulating a theory that integrates thermodynamics with quantum mechanics, which has come to be known as quantum thermodynamics [1, 2]. Several studies in this area focus on investigating the so-called quantum heat engines: heat engines in which the working substance is a quantum system [3–44]. When studying quantum heat engines, a natural question is whether quantum resources can improve their performance. Addressing this question, Ref. [11] revealed that a quantum Otto heat engine (QOHE) with a quantum harmonic oscillator as its working substance can achieve higher efficiencies when, instead of a conventional thermal reservoir (a heat reservoir with a positive temperature), its heat source is a squeezed thermal reservoir. Furthermore, the authors showed that the efficiency of the corresponding QOHE can surpass the Carnot efficiency obtained from the temperatures of the thermal reservoirs before squeezing the hottest one, which is the maximum efficiency achievable by a heat engine operating solely with thermal reservoirs. Following this, Ref. [19] presented an experimental realization of such a QOHE. Employing a two-level system as the working substance, Ref. [37] demonstrated that a squeezed thermal reservoir can increase the efficiency of the QOHE beyond the Carnot efficiency (before squeezing) even when it operates with irreversible unitary strokes. Here we are referring to the concept of irreversibility from quantum thermodynamics perspective, see Ref. [45]. Using the same working substance but now considering a heat reservoir with an apparent negative temperature as the heat source, Ref. [28] showed that the efficiency of the QOHE can exceed the Otto efficiency when the unitary strokes are irreversible. The potential of using different types of heat reservoirs to improve engine efficiency is the motivation of the present paper.

We present in this paper a scheme that employs an ion confined in a bi-dimensional trap to simulate QOHE whose working substance is a two-level system. The proposed scheme allows the two-level system to operate with

different kinds of effective heat reservoirs. Here we focus on effective thermal reservoirs, effective heat reservoirs with apparent negative temperatures, and effective squeezed thermal reservoirs. We begin in Sec. II by describing the physical model employed to simulate the QOHE whose working substance is the two-level system. Then, in Secs. III and IV, we provide an overview of the unitary and non-unitary strokes that give rise to the quantum Otto cycle. In Sec. IV, we present the procedure for generating the effective heat reservoirs for the two-level system. Next, in Sec. V, we describe the quantum Otto cycle and provide the engine efficiency when it operates as a heat engine. In Sec. VI, we show some numerical results. Additionally, in Sec. VII, we discuss the simulation of a QOHE with a quantum harmonic oscillator as the working substance, considering the same types of effective heat reservoirs as above. Finally, in Sec. VIII, we present our conclusions.

II. PHYSICAL MODEL

The physical model we consider here consists of an ion within a bi-dimensional trap that enables it to oscillate harmonically along both the x and y axes. We assume that two energy levels approximately describe the electronic structure of the ion and the transition frequency between them can vary in time. Furthermore, we admit that the ion can interact (through its dipole moment) with the electric field of four distinct laser beams: two propagating in the x direction and two in the y direction. The Hamiltonian that describes this system at time t has the form

$$H(t) = H_e(t) + H_m + H_{int}(t), \quad (1)$$

with $H_e(t)$, H_m , and $H_{int}(t)$ being the electronic, the motional, and the interaction Hamiltonian, respectively. Explicitly, the Hamiltonians $H_e(t)$ and H_m are given by

$$H_e(t) = \frac{\hbar\omega_e(t)}{2}\sigma_z \quad (2)$$

and

$$H_m = \sum_{\alpha=x,y} \hbar \omega_m a_\alpha^\dagger a_\alpha, \quad (3)$$

where $\omega_e(t)$ is the electronic frequency, σ_z is the z -Pauli matrix, ω_m is the motional frequency of the ion along the x and y axes (assumed the same for both modes, for simplicity), and a_α (a_α^\dagger) is the respective annihilation (creation) operator, with α being x or y . In turn, the interaction Hamiltonian can be written as [46]

$$H_{int}(t) = \sum_{\alpha=x,y} \sum_{l=1}^2 \frac{\hbar \Omega_{\alpha,l}}{2} (\sigma_{ge} + \sigma_{ge}^\dagger) \times \left\{ e^{i[\lambda(a_\alpha + a_\alpha^\dagger) - \omega_{\alpha,l}^L t + \phi]} + \text{H.c.} \right\}, \quad (4)$$

where $\Omega_{\alpha,l}$ is the Rabi frequency, $\sigma_{ge} = |g\rangle\langle e|$ ($\sigma_{ge}^\dagger = |e\rangle\langle g|$) is the lowering (raising) operator, with $|g\rangle$ ($|e\rangle$) corresponding to the fundamental (excited) electronic eigenstate, λ is the Lamb-Dicke parameter, $\omega_{\alpha,l}^L$ is the laser frequency, and ϕ is the initial phase of the lasers. Note that, for simplicity, we are considering the same Lamb-Dicke parameter and initial phase for all lasers. We assume that the dynamics of the ion density matrix $\rho(t)$ is that of a weak interaction with the reservoir within the Born-Markov approximations, and therefore obeys the master equation

$$\dot{\rho}(t) = \frac{1}{i\hbar} [H(t), \rho(t)] + \sum_{\alpha=x,y} \frac{\kappa}{2} D[a_\alpha] \rho(t), \quad (5)$$

in which κ is the motional decay rate (also considered the same for the x and y directions, for simplicity) and $D[a_\alpha] \rho(t) = 2a_\alpha \rho(t) a_\alpha^\dagger - a_\alpha^\dagger a_\alpha \rho(t) - \rho(t) a_\alpha^\dagger a_\alpha$. As can be seen, we are neglecting the electronic decay, which is a reasonable assumption when it is significantly smaller than κ .

III. UNITARY STROKE

After introducing the physical model, we move on to describe the evolution of the two-level system throughout the strokes of the quantum Otto cycle, beginning with the unitary strokes. In these strokes, the electronic component of the ion (ECI) evolves unitarily while its frequency changes from an initial value $\omega_e(0)$ to a final value $\omega_e(\tau)$ according to time-dependent function $\omega_e(t)$. For instance, this can be achieved by applying an external magnetic field on the trapped ion [47]. When the electronic frequency increases, the unitary stroke is called an expansion stroke; otherwise, it is called a compression stroke. Assuming that the trapped ion does not interact with any field capable to induce transitions during the frequency change, it follows from Eqs. (1) and (5) that its electronic component undergoes a unitary evolution.

In this case, therefore, the dynamics of the electronic state $\rho_e(t) = \text{tr}_m[\rho(t)]$ obeys the von Neumann equation

$$\dot{\rho}_e(t) = \frac{1}{i\hbar} [H_e(t), \rho_e(t)]. \quad (6)$$

Consequently, the ECI goes from the initial state $\rho_e(0)$ to the final state $\rho_e(\tau) = U_{e,1}(\tau) \rho_e(0) U_{e,1}(\tau)^\dagger$, in which the unitary evolution operator has the form $U_{e,1}(\tau) = e^{-(i/\hbar) \int_0^\tau dt H_e(t)}$.

By examining Eq. (2), it is straightforward to see that $[H_e(t), H_e(t')] = 0$ for any t and t' , regardless of the chosen time-dependent function $\omega_e(t)$. This feature ensures that the unitary stroke described above does not induce transitions between the electronic states $|g\rangle$ and $|e\rangle$, as can be comprehended by noting that $\langle g | \rho_e(\tau) | g \rangle = \langle g | U_{e,1}(\tau) \rho_e(0) U_{e,1}(\tau)^\dagger | g \rangle = \langle g | \rho_e(0) | g \rangle$. In most cases, transitions between these states are undesirable since they are associated with entropy production (irreversibility) [45], which usually reduces engine efficiency. For instance, this applies to the QOHE in which a two-level system operates with two thermal reservoirs [27] as well as its modified version where the hot thermal reservoir is replaced by a squeezed one [37]. In contrast, transitions in the unitary strokes are advantageous when the two-level system operates with the hot heat reservoir at apparent negative temperatures, as they have the potential to enhance engine efficiency [28]. Thus, it is interesting to improve the unitary stroke presented above to account for situations involving such transitions.

To promote transitions between $|g\rangle$ and $|e\rangle$, we introduce an additional unitary evolution immediately after the one described above, with a duration of τ' . In this new step, while keeping the electronic frequency at $\omega_e(\tau)$, we enable the ion to interact with the electric field of a laser beam propagating in the x direction with frequency $\omega_{x,1}^L = \omega_e(\tau)$. By eliminating the summations in Eq. (4) (setting $\alpha = x$ and $l = 1$), considering the Lamb-Dicke regime, which means $\lambda [\text{tr}_m(a_x^\dagger a_x)]^{1/2} \ll 1$, and choosing $\phi = 0$, the rotating-wave approximation leads to the interaction Hamiltonian [46]

$$H_{int}(t) = \frac{\hbar \Omega}{2} \left[\sigma_- e^{i\omega_e(\tau)t} + \sigma_+ e^{-i\omega_e(\tau)t} \right], \quad (7)$$

where $\Omega \equiv \Omega_{x,1}$. Therefore, the ECI evolves unitarily according to Eq. (5) but with Hamiltonian $H_e(\tau) + H_{int}(t)$. Consequently, the electronic state goes from $\rho_e(\tau)$ to $\rho_e(\tau + \tau') = U_{e,2}(\tau') \rho_e(\tau) U_{e,2}(\tau')^\dagger$, where $U_{e,2}(\tau') = T_+ e^{-(i/\hbar) \int_\tau^{\tau+\tau'} dt [H_e(\tau) + H_{int}(t)]}$, with T_+ being the time-ordering operator. Note that the desired transitions are now attainable since $[H_e(\tau) + H_{int}(t), H_e(\tau) + H_{int}(t')] \neq 0$ for any t and t' such that $t' \neq t$. The transition probability between the electronic states is given by

$$\xi(\tau') = |\langle e | U_{e,2}(\tau') | g \rangle|^2. \quad (8)$$

As it can be seen, we can control the transition probability by adjusting the time the laser beam acts on the ion, denoted as τ' .

Lastly, we can condense the two unitary evolutions presented previously into the unitary evolution operator $U_e(\tau+\tau')=U_{e,2}(\tau')U_{e,1}(\tau)$, which transforms $\rho_e(0)$ into $\rho_e(\tau+\tau')=U_e(\tau+\tau')\rho_e(0)U_e^\dagger(\tau+\tau')$.

IV. NON-UNITARY STROKE

Now, we proceed to describe the non-unitary strokes, which involve the thermalization process between the ECI and a specified effective heat reservoir. During these strokes, we maintain the electronic frequency constant while allowing the ion to interact, in addition to the dissipation channels for the vibrational modes, with a specific set of laser beams, which gives rise to the desired effective heat reservoir for its electronic component. Below, we describe the procedure to generate effective reservoirs such as (i) an effective thermal reservoir, (ii) an effective heat reservoir with an apparent negative temperature, and (iii) an effective squeezed thermal reservoir. We begin by addressing the effective squeezed thermal reservoir, which makes it easier to approach the remaining effective heat reservoirs.

To generate the effective squeezed thermal reservoir, we assume that the ion interacts with the four laser beams introduced in Sec. II, see Eq. (4). Additionally, we set their frequencies as follows: $\omega_{\alpha,1}^L=\omega_e-\omega_m$ and $\omega_{\alpha,2}^L=\omega_e+\omega_m$ ($\alpha=x,y$), where ω_e is a short notation for $\omega_e(0)$ or $\omega_e(\tau)$ from Sec. III. In this case, restricting to the Lamb-Dicke regime, applying the rotating-wave approximation, and fixing $\phi=-\pi/2$, the interaction Hamiltonian of (Eq. (4)) becomes

$$H_{int}(t)=\sum_{\alpha=x,y}\hbar[s_\alpha(t)a_\alpha^\dagger e^{-i\omega_m t}+s_\alpha^\dagger(t)a_\alpha e^{i\omega_m t}], \quad (9)$$

with

$$s_\alpha(t)=\frac{\lambda}{2}(\Omega_{\alpha,1}\sigma_{ge}e^{i\omega_e t}+\Omega_{\alpha,2}\sigma_{ge}^\dagger e^{-i\omega_e t}). \quad (10)$$

Then, taking into account Eq. (9) in Eq. (5), assuming $\kappa\gg\lambda\Omega_{\alpha,l}$ so that $\rho(t)\approx(\prod_{\alpha=x,y}|0_\alpha\rangle\langle 0_\alpha|)\rho_e(t)$, where $|0_\alpha\rangle$ is the motional ground state in the α direction, and tracing over the motional degrees of freedom, we can employ the adiabatic elimination (as detailed in the first section of the Supplementary Material) [48] to obtain the effective master equation

$$\dot{\rho}_e(t)=\frac{1}{i\hbar}[H_e,\rho_e(t)]+\sum_{\alpha=x,y}\frac{2}{\kappa}D[s_\alpha(t)]\rho_e(t), \quad (11)$$

in which H_e represents either $H_e(0)$ or $H_e(\tau)$, depending on the stroke considered.

Now that we have Eq. (11) at our disposal, it remains to compare it with the master equation derived by considering a squeezed thermal reservoir to adjust our parameters accordingly. Explicitly, we must compare Eq.

(11) with the master equation [49]

$$\dot{\rho}_e(t)=\frac{1}{i\hbar}[H_e,\rho_e(t)]+\sum_{i=1}^2\frac{1}{2}D[R_i(t)]\rho_e(t), \quad (12)$$

in which

$$R_1(t)=\sqrt{\gamma(1+n_R)}(\mu\sigma_{ge}e^{i\omega_e t}+\nu\sigma_{ge}^\dagger e^{-i\omega_e t}), \quad (13)$$

and

$$R_2(t)=\sqrt{\gamma n_R}(\nu\sigma_{ge}e^{i\omega_e t}+\mu\sigma_{ge}^\dagger e^{-i\omega_e t}). \quad (14)$$

Here, γ is the electronic decay rate (related to the coupling of the ion to a squeezed thermal reservoir), n_R is the average number of photons in the thermal reservoir before squeezing (which follows from the Bose-Einstein distribution), $\mu=\cosh(r)$, and $\nu=\sinh(r)$, with r being the squeezing parameter. Upon comparing Eq. (11) with Eq. (12), it becomes evident that if we chose

$$\frac{\lambda\Omega_{x,1}}{\sqrt{\kappa}}=\sqrt{\gamma(1+n_R)}\mu, \quad (15)$$

$$\frac{\lambda\Omega_{x,2}}{\sqrt{\kappa}}=\sqrt{\gamma(1+n_R)}\nu, \quad (16)$$

$$\frac{\lambda\Omega_{y,1}}{\sqrt{\kappa}}=\sqrt{\gamma n_R}\nu, \quad (17)$$

and

$$\frac{\lambda\Omega_{y,2}}{\sqrt{\kappa}}=\sqrt{\gamma n_R}\mu, \quad (18)$$

we ensure that Eq. (11) reproduces the dynamics of a two-level system weakly coupled to a squeezed thermal reservoir.

Before proceeding to the remaining effective heat reservoirs, it is worthwhile to show the state that the ECI reaches when equilibrating with the effective squeezed thermal reservoir. By solving Eq. (12) and taking $t\rightarrow\infty$, we obtain the steady-state [49]

$$\rho_e^S=S\rho_e^G S^\dagger, \quad (19)$$

in which ρ_e^G is the so-called Gibbs state, and S is a unitary operator such that

$$S|g\rangle\langle g|S^\dagger=\frac{1}{\mu^2+\nu^2}(\mu^2|g\rangle\langle g|+\nu^2|e\rangle\langle e|), \quad (20)$$

and

$$S|e\rangle\langle e|S^\dagger=\frac{1}{\mu^2+\nu^2}(\nu^2|g\rangle\langle g|+\mu^2|e\rangle\langle e|). \quad (21)$$

The Gibbs state has the form

$$\rho_e^G=\frac{e^{-\beta_R H_e}}{Z_e}, \quad (22)$$

where $\beta_R=1/(k_B T_R)$, with T_R being the temperature of the thermal reservoir before squeezing, and $Z_e=\text{tr}(e^{-\beta_R H_e})$. So, if Eqs. (15)-(18) are satisfied, ρ_e^S is the electronic state after equilibration.

We now address the effective thermal reservoir either at positive or apparent negative temperatures. The procedure we follow here is similar to the one performed above: we compare Eq. (11) with the master equation obtained by considering the desired heat reservoir, aiming to identify the conditions that make these equations identical. The master equation we must compare with Eq. (11) follows the same structure as Eq. (12) but with operators [50, 51]

$$R_1 = \sqrt{\gamma(1 \pm n_R)} \sigma_{ge} \quad (23)$$

and

$$R_2 = \sqrt{\gamma n_R} \sigma_{ge}^\dagger. \quad (24)$$

In Eq. (24), we apply the positive sign if $n_R = 1/(e^{\beta_R \hbar \omega_e} - 1)$, following the Bose-Einstein distribution ($n_R \in (0, \infty)$), and the negative sign if $n_R = 1/(e^{\beta_R \hbar \omega_e} + 1)$, following the Fermi-Dirac distribution ($n_R \in (0, 1)$). When n_R corresponds to the Fermi-Dirac distribution and $n_R \in (1/2, 1)$, $\beta_R < 0$; for $n_R \in (0, 1/2)$, $\beta_R > 0$. Therefore, when we consider R_1 and R_2 as defined by Eqs. (23) and (24), Eq. (12) covers both master equations corresponding to a thermal reservoir ($\beta_R > 0$) and a heat reservoir with an apparent negative temperature ($\beta_R < 0$). Then, by comparing this equation with Eq. (11), we obtain

$$\frac{\lambda \Omega_{x,1}}{\sqrt{\kappa}} = \sqrt{\gamma(1 \pm n_R)}, \quad (25)$$

$$\frac{\lambda \Omega_{x,2}}{\sqrt{\kappa}} = 0, \quad (26)$$

$$\frac{\lambda \Omega_{y,1}}{\sqrt{\kappa}} = 0, \quad (27)$$

and

$$\frac{\lambda \Omega_{y,2}}{\sqrt{\kappa}} = \sqrt{\gamma n_R}. \quad (28)$$

Thus, if we configure the laser beams to satisfy Eqs. (25)-(28), Eq. (11) reproduces the dynamics of a two-level system in contact with a thermal reservoir, either at positive or at apparent negative temperatures. As it is well known, under the conditions above the steady-state of Eq. (11) is the Gibbs state displayed in Eq. (22), with $\beta_R > 0$ or $\beta_R < 0$, depending on R_1 and R_2 .

V. QUANTUM OTTO HEAT ENGINE

We begin this section by describing the quantum Otto cycle corresponding to the QOHE we are interested in

simulating. As previously mentioned, our goal here is to simulate in the context of trapped ions a QOHE whose working substance is a two-level system operating between a cold and a hot heat reservoir. We assume that the cold heat reservoir is always a thermal reservoir. On the other hand, the hot heat reservoir can be a thermal reservoir, a heat reservoir with an apparent negative temperature, or a squeezed thermal reservoir. As discussed previously, the two-level system corresponds to the ECI, which can effectively interact with these reservoirs. To facilitate the exposition, we initially describe the quantum Otto cycle with an effective squeezed thermal reservoir as its hot heat reservoir. The strokes that constitute the quantum Otto cycle are as follows (see Fig. 1):

Expansion stroke. In this first stroke, the ECI undergoes the unitary evolution described by $U_e^{exp}(\tau + \tau') = U_{e,2}^{exp}(\tau') U_{e,1}^{exp}(\tau)$, where $U_{e,1}^{exp}(\tau)$ and $U_{e,2}^{exp}(\tau')$ correspond to the operators $U_{e,1}(\tau)$ and $U_{e,2}(\tau')$ introduced in Sec. II, with $\omega_e(0) = \omega_e^c$ and $\omega_e(\tau) = \omega_e^h$ ($\omega_e^h > \omega_e^c$). At the beginning of this stroke, the ECI is in the Gibbs state $\rho_e^{G,c} = e^{-\beta_R^c H_e^c} / Z_e^c$, in which $\beta_R^c = 1/k_B T_R^c$, with T_R^c being the temperature of the effective cold thermal reservoir, $H_e^c = \hbar \omega_e^c \sigma_z / 2$, and $Z_e^c = \text{tr}(e^{-\beta_R^c H_e^c})$. Note that the superscript ‘‘c’’ denotes that we are referring to the effective cold heat reservoir. Then, the electronic state at the end of the unitary evolution is $\rho_e^{exp}(\tau') = U_{e,2}^{exp}(\tau') \rho_e^{G,c} U_{e,1}^{exp}(\tau)^\dagger$, as $U_{e,1}^{exp}(\tau)$ does not modify the electronic state (since $[U_{e,1}^{exp}(\tau), \rho_e^{G,c}] = 0$).

Heating stroke. At this stroke, the ECI evolves non-unitarily by interacting effectively with the squeezed hot thermal reservoir, as addressed in Sec. IV. Therefore, the dynamics of the electronic state is governed by Eq. (11), with the parameters meeting the conditions specified in Eqs. (15)-(18). To explicitly indicate that we are dealing with the effective hot heat reservoir, we use the superscript ‘‘h’’ in these equations, resulting in the notation changes $H_e \rightarrow H_e^h = \hbar \omega_e^h \sigma_z / 2$, $s_\alpha(t) \rightarrow s_\alpha^h(t) = \lambda(\Omega_{\alpha,1}^h \sigma_- e^{i\omega_e^h t} + \Omega_{\alpha,2}^h \sigma_+ e^{-i\omega_e^h t}) / 2$, and $n_R \rightarrow n_R^h$. The stroke ends when the ECI equilibrates with the effective hot heat reservoir, reaching the steady-state $\rho_e^{S,h} = S \rho_e^{G,h} S^\dagger$, where $\rho_e^{G,h} = e^{-\beta_R^h H_e^h} / Z_e^h$. Here, $\beta_R^h = 1/k_B T_R^h$, with T_R^h being the temperature of the hot thermal reservoir before squeezing, and $Z_e^h = \text{tr}(e^{-\beta_R^h H_e^h})$.

Compression stroke. During this stroke, the electronic state evolves unitarily according to $U_e^{comp}(\tau + \tau') = U_{e,2}^{comp}(\tau') U_{e,1}^{comp}(\tau)$, where $U_{e,1}^{comp}(\tau)$ and $U_{e,2}^{comp}(\tau')$ match the operators $U_{e,1}(\tau)$ and $U_{e,2}(\tau')$ from Sec. II, observing that $\omega_e(0) = \omega_e^h$ and $\omega_e(\tau) = \omega_e^c$. As a result, the present stroke leads the ECI to the state $\rho_e^{comp}(\tau') = U_{e,2}^{comp}(\tau') \rho_e^{S,h} U_{e,1}^{comp}(\tau)^\dagger$.

Cooling stroke. As a final stroke, the ECI interacts effectively with the cold thermal reservoir until thermalization. Here, as discussed in Sec. IV, the electronic state undergoes a non-unitary evolution dictated by Eq. (11), obeying Eqs. (25)-(28). To explicitly denote that

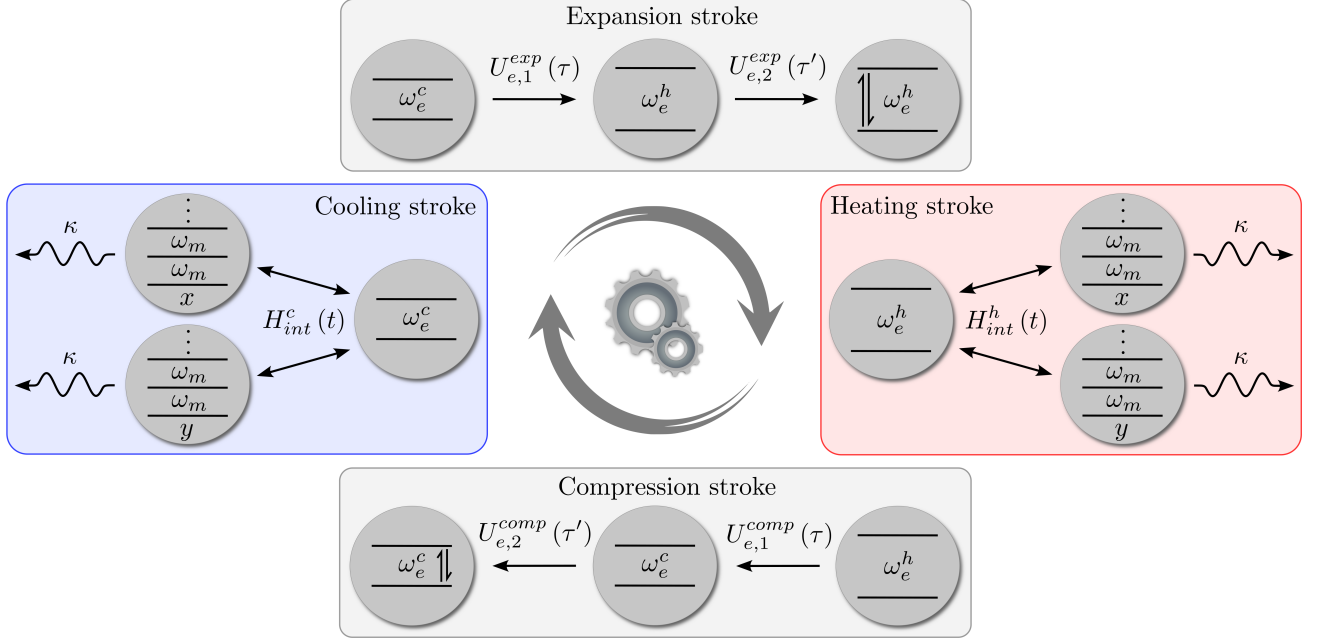


Figure 1. Scheme displaying the quantum Otto cycle described in the text. The boxes represent the cycle strokes. Starting with the cooling stroke, ω_e^c corresponds to the electronic frequency of the ion, ω_m represents the motional frequency of the ion in the x and y directions, κ denotes the motional decay rate, and $H_{int}^c(t)$ stands for the interaction Hamiltonian between the electronic and motional components of the ion. As the text explains, $H_{int}^c(t)$ determines the effective cold heat reservoir for the electronic component of the ion (ECI). In the expansion stroke, the two-level system undergoes a unitary evolution dictated by $U_{e,1}^{exp}(\tau)$, which causes the energy gap expansion $\omega_e^c \rightarrow \omega_e^h$ ($\omega_e^h > \omega_e^c$) after the time τ . Next, the unitary evolution $U_{e,2}^{exp}(\tau')$ induces transitions in the ECI during the interval τ' , represented by the vertical arrows between the electronic energy levels. Moving on to the heating stroke, the interaction Hamiltonian is now $H_{int}^h(t)$, which leads to the effective hot heat reservoir for the ECI. Finally, in the compression stroke, the unitary operator $U_{e,1}^{comp}(\tau)$ compresses the energy gap of the ECI, and $U_{e,2}^{comp}(\tau')$ induces transitions between its energy levels.

we are referring to the effective cold heat reservoir, we introduce the superscript “ c ” in these equations, leading to the notation modifications $H_e \rightarrow H_e^c$, $s_\alpha(t) \rightarrow s_\alpha^c(t) = \lambda(\Omega_{\alpha,1}^c \sigma_- e^{i\omega_e^c t} + \Omega_{\alpha,2}^c \sigma_+ e^{-i\omega_e^c t})/2$, and $n_R \rightarrow n_R^c$. When the thermalization occurs, the ECI reaches the Gibbs state $\rho_e^{G,c}$, thus closing the cycle.

After describing the cycle, we can proceed to determine the engine efficiency. For this purpose, we first calculate the heat and work associated with each cycle stroke. To obtain these quantities, we adopt the following definitions for work and heat [52, 53]: $W_e^{str} = \int_{t_i}^{t_f} dt \text{tr}[\dot{H}_e^{str}(t) \rho_e^{str}(t)]$ and $Q_e^{str} = \int_{t_i}^{t_f} dt \text{tr}[H_e^{str}(t) \dot{\rho}_e^{str}(t)]$. Here, $H_e^{str}(t)$ and $\rho_e^{str}(t)$ correspond to the Hamiltonian and the state that describe the ECI throughout the respective strokes. With these definitions, it is straightforward to show that the expansion and compression strokes involve only work (W_e^{comp} and W_e^{exp}), whereas the heating and cooling strokes involve solely heat (Q_e^h and Q_e^c). Thus, by calculating the energy exchanged in each stroke,

we obtain the net work ($W_e^{net} = W_e^{exp} + W_e^{comp}$)

$$W_e^{net} = -\frac{\hbar(\omega_e^h - \omega_e^c)}{2} [\tanh(\theta^c) - \zeta \tanh(\theta^h)] + \hbar\xi [\omega_e^h \tanh(\theta^c) + \omega_e^c \tanh(\theta^h)], \quad (29)$$

the heat associated with the heating stroke

$$Q_e^h = \frac{\hbar\omega_e^h}{2} [\tanh(\theta^c) - \zeta \tanh(\theta^h) - 2\xi \tanh(\theta^c)], \quad (30)$$

and the heat linked to the cooling stroke

$$Q_e^c = -\frac{\hbar\omega_e^c}{2} [\tanh(\theta^c) - \zeta \tanh(\theta^h) + 2\xi \tanh(\theta^h)], \quad (31)$$

where $\theta^{c(h)} = \beta_R^{c(h)} \hbar\omega_e^{c(h)}/2$ and $\zeta = 1/(\mu^2 + \nu^2)$, as derived in Ref. [37]. For the sake of simplicity, we are omitting the time dependence of the probability transition ($\xi = \xi(\tau')$).

The condition for the cycle presented above to operate as a heat engine is $W_e^{net} < 0$, indicating the extraction of net work from the ECI after the four strokes. If this condition is satisfied, the engine efficiency η is determined using the formula

$$\eta = -\frac{W_e^{net}}{Q_e^{abs}}, \quad (32)$$

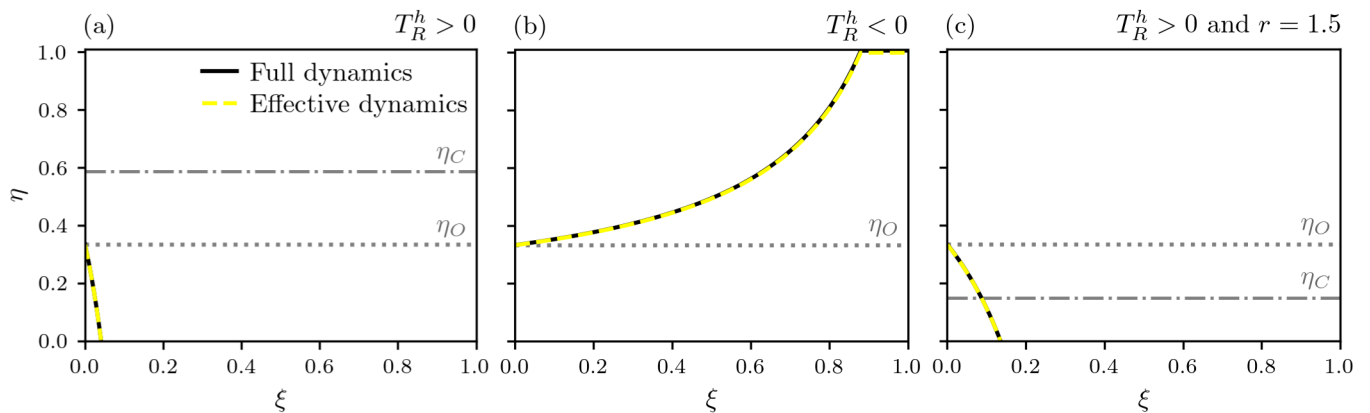


Figure 2. Engine efficiency η as a function of the transition probability ξ . Panel (a) displays curves associated with the effective hot thermal reservoir, panel (b) shows curves related to the effective hot reservoir with an apparent negative temperature, and panel (c) depicts curves linked with the effective hot squeezed thermal reservoir. In panels (a)-(c), we assume a cold thermal reservoir with $n_R^c=0.6$, defined by the Bose-Einstein distribution. In panel (a), we choose $n_R^h=1.2$, determined by the Bose-Einstein distribution; in panel (b), $n_R^h=0.8$, given by the Fermi-Dirac distribution; and in panel (c), $n_R^h=0.4$, provided by the Bose-Einstein distribution. In addition, we set $\omega_e^c=2\pi$ THz, $\omega_e^h=3\pi$ THz, $\omega_m=20\pi$ MHz, $\lambda=10^{-2}$, $\Omega=20\pi$ kHz, $\kappa=2\pi$ MHz $^{-1}$, and $\gamma=2\pi\times 10^{-1}$ kHz $^{-1}$. The yellow dashed lines correspond to the case in which we apply the adiabatic elimination in the heating and cooling strokes (effective dynamics), the black solid lines correspond to the situation in which we do not perform the adiabatic elimination (full dynamics), the gray dotted lines show the Otto efficiency η_O , and the gray dot-dashed lines display the Carnot efficiency η_C .

with Q_e^{abs} representing the heat absorbed by the ECI ($Q_e^{abs}>0$) during the cycle. Considering Eqs. (29)-(31), it is easy to demonstrate that $W_e^{net}<0$ implies $Q_e^h>0$ and $Q_e^c<0$, resulting in $Q_e^{abs}=Q_e^h$. As a result, the engine efficiency can be expressed as [37]

$$\eta^S = 1 - \frac{\omega_e^c}{\omega_e^h} \left[\frac{\tanh(\theta^c) - (1-2\xi)\zeta \tanh(\theta^h)}{(1-2\xi)\tanh(\theta^c) - \zeta \tanh(\theta^h)} \right]. \quad (33)$$

As stated in Ref. [37], η^S cannot surpass the Otto efficiency $\eta_O = 1 - \omega_e^c/\omega_e^h$ but can exceed the Carnot efficiency $\eta_C = 1 - \beta_R^h/\beta_R^c$. This is because the squeezing process actually adds photons into the hot heat reservoir, increasing its effective temperature when compared to its initial temperature T_R^h .

We can now easily adjust the cycle and expressions introduced above to account for the cases where the QOHE operates with a thermal reservoir and a heat reservoir with an apparent negative temperature as its hot heat reservoir. The adjustment in the cycle involves allowing the ECI to interact effectively with one of these heat reservoirs, which changes the final electronic state of the heating stroke and, consequently, the initial and final electronic states of the compression stroke. Thus, the ECI attains a Gibbs state (Eq. (22)) at the end of the heating stroke, with $\beta_R^h>0$ for the effective hot thermal reservoir and $\beta_R^h<0$ for the effective hot heat reservoir with an apparent negative temperature. Subsequently, we obtain the final electronic state of the compression stroke by applying $U_{e,2}^{comp}(\tau')$ to the respective Gibbs state. As a result, we can rewrite Eqs. (29)-(31) by taking $r=0$ (which implies $S=I$ and $\zeta=1$) and, if we are considering an effective hot heat reservoir with an

apparent negative temperature, $\beta_R^h = -|\beta_R^h|$ ($\theta^h = -|\theta^h|$). In the case involving an effective hot thermal reservoir, $W_e^{net}<0$ then results in $Q_e^h>0$ and $Q_e^c<0$ ($Q_e^{abs}=Q_e^h$), allowing us to express the engine efficiency as [27]

$$\eta^+ = 1 - \frac{\omega_e^c}{\omega_e^h} \left[\frac{\tanh(\theta^c) - (1-2\xi)\tanh(\theta^h)}{(1-2\xi)\tanh(\theta^c) - \tanh(\theta^h)} \right]. \quad (34)$$

On the other hand, in the case involving an effective hot heat reservoir with an apparent negative temperature, $W_e^{net}<0$ does not always imply $Q_e^h>0$ and $Q_e^c<0$; there are values of ξ that yield $Q_e^h>0$ and $Q_e^c>0$. If the ECI absorbs heat from both effective heat reservoirs, $\eta^- = 1$, whereas if it absorbs heat only from the effective hot heat reservoir [28],

$$\eta^- = 1 - \frac{\omega_e^c}{\omega_e^h} \left[\frac{\tanh(\theta^c) + (1-2\xi)\tanh(|\theta^h|)}{(1-2\xi)\tanh(\theta^c) + \tanh(|\theta^h|)} \right]. \quad (35)$$

As discussed in Ref. [28], the hot heat reservoir with an apparent negative temperature can lead to $\eta^- > \eta_O$, depending on the value of ξ .

VI. NUMERICAL RESULTS

In this section, we present some numerical results that illustrate the effectiveness of the proposed scheme in simulating the QOHE of interest. For this purpose, we numerically replicate the cycles described in the previous section, considering both the scenario in which we perform the adiabatic elimination (in the heating and cooling strokes) and the one where we do not. By applying

this approximation, we obtain the dynamics of the ECI utilizing Eq. (11); otherwise, we use Eq. (5) with the interaction Hamiltonian provided by Eq. (9). In this way, we can verify the accuracy of the adiabatic elimination, which gives rise to the desired effective dynamics during the heating and cooling strokes. Furthermore, while ensuring the Lamb-Dicke regime and the validity of the rotating wave approximation, we select parameters of the same order as those observed in experimental setups involving trapped ions [46, 54, 55]. We obtain the numerical results using the Quantum Toolbox in Python (QuTiP) [56, 57].

The numerical results are shown in Figs. 2(a)-(c), where we display the engine efficiency η as a function of the transition probability ξ . Fig. 2(a) corresponds to the case involving an effective hot thermal reservoir (η^+), Fig. 2(b) to the situation involving an effective hot heat reservoir with an apparent negative temperature (η^-), and Fig. 2(c) to the scenario involving an effective squeezed hot thermal reservoir (η^S). In these figures, we set $\omega_e^c = 2\pi$ THz, $\omega_e^h = 3\pi$ THz, $\omega_m = 20\pi$ MHz, $\lambda = 10^{-2}$, $\Omega = 20\pi$ kHz, $\kappa = 2\pi$ MHz $^{-1}$, $\gamma = 2\pi \times 10^{-1}$ kHz $^{-1}$, and $n_R^c = 0.6$ (given by the Bose-Einstein distribution). Additionally, we assume $n_R^h = 1.2$ (provided by the Bose-Einstein distribution) in Fig. 2(a), $n_R^h = 0.8$ (given by the Fermi-Dirac distribution) in Fig. 2(b), and $n_R^h = 0.4$ (determined by the Bose-Einstein distribution) in Fig. 2(c). With these quantities, it is straightforward to calculate the respective Rabi frequencies $\Omega_{x,1}^{c(h)}$, $\Omega_{x,2}^{c(h)}$, $\Omega_{y,1}^{c(h)}$, and $\Omega_{y,2}^{c(h)}$ by using Eqs. (15)-(18) or (25)-(28), depending on the case. Therefore, since the parameters are adjusted to reproduce the desired dynamics, it remains solely to verify the validity of the approximations employed to obtain the effective dynamics. In Figs. 2(a)-(c), the yellow dashed lines correspond to the case in which we perform the adiabatic elimination (effective dynamics), derived in detail in the first section of the Supplementary Material, while the solid black lines are associated with the scenario in which we do not perform such an approximation (full dynamics). Besides, the gray dotted and dot-dashed lines indicate the corresponding Otto and Carnot efficiencies, respectively. As we can see, the yellow dashed lines overlap the black solid ones, thus illustrating the validity of the adiabatic elimination applied to derive Eq. (12).

VII. HOW ABOUT A QUANTUM HARMONIC OSCILLATOR AS THE WORKING SUBSTANCE?

Having addressed the case involving a two-level system as the working substance, we now briefly discuss the simulation of a QOHE that has a quantum harmonic oscillator as the working substance. To simulate such a QOHE, considering the different types of heat reservoirs discussed previously, we need a physical model different from the one presented in Sec. II. Here, considering only the oscillation of the ion in a given direction, assuming that three energy levels in the V configuration define its

electronic structure, and allowing it to interact with a set of four laser beams (as in Sec. II), the Hamiltonian that describes the ion is

$$H(t) = H_e + H_m + H(t), \quad (36)$$

with

$$H_e = \frac{\hbar\omega_{ge}}{2}|e\rangle\langle e| + \frac{\hbar\omega_{gf}}{2}|f\rangle\langle f|, \quad (37)$$

$$H_m = \hbar\omega_m a^\dagger a, \quad (38)$$

and

$$H_{int}(t) = \sum_{\alpha=ge,gf} \sum_{l=1}^2 \frac{\hbar\Omega_{\alpha,l}}{2} (\sigma_\alpha + \sigma_\alpha^\dagger) \times \left\{ e^{i[\lambda(a+a^\dagger) - \omega_{\alpha,l}^L t + \phi]} + \text{H.c.} \right\}. \quad (39)$$

In Eq. (37), $|e\rangle$ and $|f\rangle$ are the excited electronic states, while ω_{ge} and ω_{gf} are the electronic transition frequencies between them and the ground state $|g\rangle$; in Eq. (39), $\sigma_{gf} = |g\rangle\langle f|$ ($\sigma_{gf}^\dagger = |f\rangle\langle g|$). Furthermore, we assume that the dynamics of the ion state is given now by the master equation

$$\dot{\rho}(t) = \frac{1}{i\hbar} [H(t), \rho(t)] + \sum_{\alpha=ge,gf} \frac{\gamma_\alpha}{2} D[\sigma_\alpha] \rho(t), \quad (40)$$

where γ_{ge} and γ_{gf} are the electronic decay rates. Here, in contrast to Sec. II, we consider that the motional decay rate is significantly smaller than the electronic decay rates. Consequently, we can safely disregard it.

Having defined the physical model, we can now describe the generation of the effective heat reservoirs of interest for the quantum harmonic oscillator. Following the same strategy as in Sec. IV, we start by setting $\omega_{\alpha,1}^L = \omega_\alpha - \omega_m$, $\omega_{\alpha,2}^L = \omega_\alpha + \omega_m$, and $\phi = -\pi/2$. As a result, the Lamb-Dicke regime and the rotating-wave approximation lead to the interaction Hamiltonian

$$H_{int}(t) = \sum_{\alpha=ge,gf} \hbar [s_\alpha(t) \sigma_\alpha^\dagger e^{-i\omega_\alpha t} + s_\alpha^\dagger(t) \sigma_\alpha e^{i\omega_\alpha t}], \quad (41)$$

in which

$$s_\alpha(t) = \frac{\lambda}{2} (\Omega_{\alpha,1} a e^{i\omega_m t} + \Omega_{\alpha,2} a^\dagger e^{-i\omega_m t}). \quad (42)$$

Then, assuming $\gamma_\alpha \gg \lambda\Omega_{\alpha,l}$ so that $\rho(t) \approx \rho_m(t)|g\rangle\langle g|$, tracing over the electronic degree of freedom, and applying the adiabatic elimination (see the second section of the Supplementary Material), we obtain the effective master equation

$$\dot{\rho}_m(t) = \frac{1}{i\hbar} [H_m, \rho_m(t)] + \sum_{\alpha=ge,gf} \frac{2}{\gamma_\alpha} D[s_\alpha(t)] \rho_m(t). \quad (43)$$

Thus, when we properly choose the Rabi frequencies, obeying similar relations to the ones of (15)-(18) and (25)-(28), Eq. (43) can effectively describe the dynamics of the quantum harmonic oscillator in contact with the heat reservoirs discussed in the previous sections.

Finally, we can implement the unitary steps of the cycle by turning off the laser beams and modifying the trap potential [14], which changes ω_m . Since changes in ω_m can cause transitions, because $[H_m(t), H_m(t')] \neq 0$ for any t and t' such that $t' \neq t$, we do not need an additional unitary step here as in the Sec. III.

VIII. CONCLUSION

We present a scheme that utilizes an ion confined within a bi-dimensional trap to simulate a quantum Otto heat engine (QOHE) with a two-level system as its working substance. Our scheme allows the electronic component of the ion (ECI), here considered as a two-level system, to interact with different types of effective heat reservoirs, including effective thermal reservoirs (effective heat reservoirs with positive temperatures), effective heat reservoirs with apparent negative temperatures, and effective squeezed thermal reservoirs. We describe how to generate these effective heat reservoirs and detail the strokes of the quantum Otto cycle. For comparison purposes, we display the efficiency of the QOHE when the ECI operates under three scenarios: (i) with two effective

thermal reservoirs, (ii) with an effective thermal reservoir and an effective heat reservoir with a negative apparent temperature, and (iii) with an effective thermal reservoir and an effective squeezed thermal reservoir. For all scenarios, we present numerical results that illustrate the applicability of our scheme by comparing the engine efficiencies obtained from the physical models with and without the adiabatic elimination, which is the primary approximation for generating the effective heat reservoirs mentioned above. Lastly, we also show how to simulate a QOHE whose working substance is a quantum harmonic oscillator operating with the effective heat reservoirs cited above.

ACKNOWLEDGMENTS

We acknowledge financial support from the following Brazilian agencies: Coordenação de Aperfeiçoamento de Pessoal de Nível Superior (CAPES), Financial code 001; National Council for Scientific and Technological Development (CNPq), Grants No. 311612/2021-0 and 301500/2018-5; São Paulo Research Foundation (FAPESP), Grants No. 2019/11999-5, No. 2021/04672-0, and No. 2022/10218-2; and Goiás State Research Support Foundation (FAPEG). This work was performed as part of the Brazilian National Institute of Science and Technology for Quantum Information (INCT-IQ/CNPq), Grant No. 465469/2014-0.

-
- [1] J. Gemmer, M. Michel, and G. Mahler, *Quantum Thermodynamics: Emergence of Thermodynamic Behavior Within Composite Quantum Systems*, 2nd ed., Lecture Notes in Physics (Springer Berlin, Heidelberg, 2009).
 - [2] F. Binder, L. Correa, C. Gogolin, J. Anders, and G. Adesso, *Thermodynamics in the Quantum Regime: Fundamental Aspects and New Directions*, 1st ed., Fundamental Theories of Physics (Springer Cham, 2019).
 - [3] T. D. Kieu, *Phys. Rev. Lett.* **93**, 140403 (2004).
 - [4] H. T. Quan, Y.-x. Liu, C. P. Sun, and F. Nori, *Phys. Rev. E* **76**, 031105 (2007).
 - [5] H. Wang, S. Liu, and J. He, *Phys. Rev. E* **79**, 041113 (2009).
 - [6] N. Linden, S. Popescu, and P. Skrzypczyk, *Phys. Rev. Lett.* **105**, 130401 (2010).
 - [7] M. O. Scully, K. R. Chapin, K. E. Dorfman, M. B. Kim, and A. Svidzinsky, *Proceedings of the National Academy of Sciences* **108**, 15097 (2011), <https://www.pnas.org/content/108/37/15097.full.pdf>.
 - [8] J. Wang, Z. Wu, and J. He, *Phys. Rev. E* **85**, 041148 (2012).
 - [9] S. Rahav, U. Harbola, and S. Mukamel, *Phys. Rev. A* **86**, 043843 (2012).
 - [10] D. Gelbwaser-Klimovsky, R. Alicki, and G. Kurizki, *Phys. Rev. E* **87**, 012140 (2013).
 - [11] J. Roßnagel, O. Abah, F. Schmidt-Kaler, K. Singer, and E. Lutz, *Phys. Rev. Lett.* **112**, 030602 (2014).
 - [12] R. Uzdin, A. Levy, and R. Kosloff, *Phys. Rev. X* **5**, 031044 (2015).
 - [13] M. Beau, J. Jaramillo, and A. Del Campo, *Entropy* **18**, 10.3390/e18050168 (2016).
 - [14] J. Roßnagel, S. T. Dawkins, K. N. Tolazzi, O. Abah, E. Lutz, F. Schmidt-Kaler, and K. Singer, *Science* **352**, 325 (2016), <https://www.science.org/doi/pdf/10.1126/science.aad6320>.
 - [15] S. Çakmak, F. Altintas, A. Gençten, and Ö. E. Müstecaplıoğlu, *The European Physical Journal D* **71**, 75 (2017).
 - [16] R. Kosloff and Y. Rezek, *Entropy* **19**, 136 (2017).
 - [17] X. L. Huang, Y. F. Shang, D. Y. Guo, Q. Yu, and Q. Sun, *Quantum Information Processing* **16**, 174 (2017).
 - [18] L.-M. Zhao and G.-F. Zhang, *Quantum Information Processing* **16**, 216 (2017).
 - [19] J. Klaers, S. Faelt, A. Imamoglu, and E. Togan, *Phys. Rev. X* **7**, 031044 (2017).
 - [20] K. Brandner, M. Bauer, and U. Seifert, *Phys. Rev. Lett.* **119**, 170602 (2017).
 - [21] W. Niedenzu, V. Mukherjee, A. Ghosh, A. G. Kofman, and G. Kurizki, *Nature Communications* **9**, 165 (2018).
 - [22] K. E. Dorfman, D. Xu, and J. Cao, *Phys. Rev. E* **97**, 042120 (2018).
 - [23] B. Xiao and R. Li, *Physics Letters A* **382**, 3051 (2018).
 - [24] B. Çakmak and Ö. E. Müstecaplıoğlu, *Phys. Rev. E* **99**, 032108 (2019).

- [25] P. A. Camati, J. F. G. Santos, and R. M. Serra, *Phys. Rev. A* **99**, 062103 (2019).
- [26] D. Türkpençe and F. Altintas, *Quantum Information Processing* **18**, 255 (2019).
- [27] J. P. S. Peterson, T. B. Batalhão, M. Herrera, A. M. Souza, R. S. Sarthour, I. S. Oliveira, and R. M. Serra, *Phys. Rev. Lett.* **123**, 240601 (2019).
- [28] R. J. de Assis, T. M. de Mendonça, C. J. Villas-Boas, A. M. de Souza, R. S. Sarthour, I. S. Oliveira, and N. G. de Almeida, *Phys. Rev. Lett.* **122**, 240602 (2019).
- [29] D. von Lindenfels, O. Gräß, C. T. Schmiegelow, V. Kaushal, J. Schulz, M. T. Mitchison, J. Goold, F. Schmidt-Kaler, and U. G. Poschinger, *Phys. Rev. Lett.* **123**, 080602 (2019).
- [30] J. Wang, J. He, and Y. Ma, *Phys. Rev. E* **100**, 052126 (2019).
- [31] M. Wiedmann, J. T. Stockburger, and J. Ankerhold, *New Journal of Physics* **22**, 033007 (2020).
- [32] J. Du, W. Shen, X. Zhang, S. Su, and J. Chen, *Phys. Rev. Res.* **2**, 013259 (2020).
- [33] S. Çakmak and F. Altintas, *Quantum Information Processing* **19**, 248 (2020).
- [34] T. Denzler and E. Lutz, *Phys. Rev. Res.* **2**, 032062 (2020).
- [35] V. Singh and O. E. Müstecaplıoğlu, *Phys. Rev. E* **102**, 062123 (2020).
- [36] Q. Bouton, J. Nettersheim, S. Burgardt, D. Adam, E. Lutz, and A. Widera, *Nature Communications* **12**, 2063 (2021).
- [37] R. J. de Assis, J. S. Sales, U. C. Mendes, and N. G. de Almeida, *Journal of Physics B: Atomic, Molecular and Optical Physics* **54**, 095501 (2021).
- [38] H. J. D. Miller, M. H. Mohammady, M. Perarnau-Llobet, and G. Guarnieri, *Phys. Rev. Lett.* **126**, 210603 (2021).
- [39] W. S. Teixeira, M. K. Keller, and F. L. Semião, *New Journal of Physics* **24**, 023027 (2022).
- [40] W. Ji, Z. Chai, M. Wang, Y. Guo, X. Rong, F. Shi, C. Ren, Y. Wang, and J. Du, *Phys. Rev. Lett.* **128**, 090602 (2022).
- [41] S. Kamimura, H. Hakoshima, Y. Matsuzaki, K. Yoshida, and Y. Tokura, *Phys. Rev. Lett.* **128**, 180602 (2022).
- [42] M. Kim, M. Scully, and A. Svidzinsky, *Nature Photonics* **16**, 669 (2022).
- [43] S. Aimet and H. Kwon, *Phys. Rev. A* **107**, 012221 (2023).
- [44] D. Das, G. Thomas, and A. N. Jordan, *Phys. Rev. A* **108**, 012220 (2023).
- [45] F. Plastina, A. Alecce, T. J. G. Apollaro, G. Falcone, G. Francica, F. Galve, N. Lo Gullo, and R. Zambrini, *Phys. Rev. Lett.* **113**, 260601 (2014).
- [46] D. Leibfried, R. Blatt, C. Monroe, and D. Wineland, *Rev. Mod. Phys.* **75**, 281 (2003).
- [47] M. H. Oliveira, G. Higgins, C. Zhang, A. Predojević, M. Henrich, R. Bachelard, and C. J. Villas-Boas, *Phys. Rev. A* **107**, 023706 (2023).
- [48] A. R. R. Carvalho, P. Milman, R. L. de Matos Filho, and L. Davidovich, *Phys. Rev. Lett.* **86**, 4988 (2001).
- [49] R. Srikanth and S. Banerjee, *Phys. Rev. A* **77**, 012318 (2008).
- [50] P. Li and B. Jia, *Phys. Rev. E* **83**, 062104 (2011).
- [51] A. Ghosh, S. S. Sinha, and D. S. Ray, *Phys. Rev. E* **86**, 011138 (2012).
- [52] R. Alicki, *Journal of Physics A: Mathematical and General* **12**, L103 (1979).
- [53] R. Kosloff, *The Journal of Chemical Physics* **80**, 1625 (1984), <https://doi.org/10.1063/1.446862>.
- [54] H. Häffner, C. Roos, and R. Blatt, *Physics Reports* **469**, 155 (2008).
- [55] R. Blatt and C. F. Roos, *Nature Physics* **8**, 277 (2012).
- [56] J. Johansson, P. Nation, and F. Nori, *Computer Physics Communications* **183**, 1760 (2012).
- [57] J. Johansson, P. Nation, and F. Nori, *Computer Physics Communications* **184**, 1234 (2013).